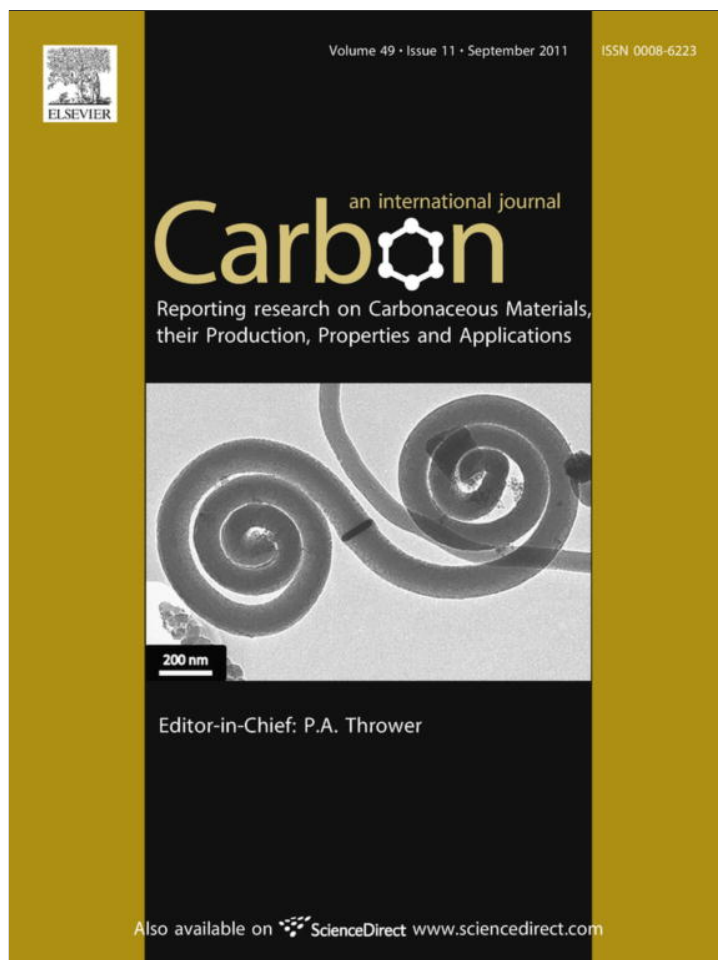


Provided for non-commercial research and education use.  
Not for reproduction, distribution or commercial use.



This article appeared in a journal published by Elsevier. The attached copy is furnished to the author for internal non-commercial research and education use, including for instruction at the authors institution and sharing with colleagues.

Other uses, including reproduction and distribution, or selling or licensing copies, or posting to personal, institutional or third party websites are prohibited.

In most cases authors are permitted to post their version of the article (e.g. in Word or Tex form) to their personal website or institutional repository. Authors requiring further information regarding Elsevier's archiving and manuscript policies are encouraged to visit:

<http://www.elsevier.com/copyright>

available at [www.sciencedirect.com](http://www.sciencedirect.com)journal homepage: [www.elsevier.com/locate/carbon](http://www.elsevier.com/locate/carbon)

# Discriminative generation and hydrogen modulation of the Dirac-Fermi polarons at graphene edges and atomic vacancies

Xi Zhang <sup>a</sup>, Yanguang Nie <sup>a</sup>, Weitao Zheng <sup>b</sup>, Jer-lai Kuo <sup>c</sup>, Chang Q. Sun <sup>a,d,\*</sup>

<sup>a</sup> School of Electrical and Electronic Engineering, Nanyang Technological University, Singapore 639798, Singapore

<sup>b</sup> School of Materials Science, Jilin University, Changchun 130012, China

<sup>c</sup> Institute of Atomic and Molecular Sciences, Academia Sinica, Taipei 10617, Taiwan

<sup>d</sup> Faculty of Materials, Photoelectronics and Physics, Xiangtan University, Changsha 400073, China

## ARTICLE INFO

### Article history:

Received 17 January 2011

Accepted 23 April 2011

Available online 29 April 2011

## ABSTRACT

Using a combination of the bond order–length–strength correlation theory, the spin-polarized tight binding method, the first-principles calculations, and the atomistic photoelectron distillation experiments, we investigated the mechanisms of edge-selective generation and hydrogenated modulation of Dirac-Fermi polarons (DFPs) surrounding the atomic vacancies at a graphite surface and at the edges of graphene nanoribbons (GNR). We found that: (i) the DFPS with a high-spin density at a zigzag-GNR edge and at an atomic vacancy result from the isolation and polarization of the dangling  $\sigma$ -bond electrons of  $\sqrt{3}d$  ( $d$  is the C–C bond length) distance along the edge by the locally and densely entrapped bonding electrons; (ii) along an armchair-GNR edge and a reconstructed-zigzag-GNR edge, however, the formation of quasi-triple-bond between the nearest edge atoms of  $d$  distance prevents the DFPS from generation; and (iii) hydrogenation reduces the spin density substantially and turns the asymmetric dumb-bell-like density into the spherical-like  $p_z$  density. A further C 1s photoelectron spectroscopic purification has confirmed that the generation of the DFPS is associated with two extra peaks of energy states located at the bottom and the top edge of the C 1s band.

© 2011 Elsevier Ltd. All rights reserved.

## 1. Introduction

As one of the allotropes of carbon, graphene with different types of edges and defects demonstrates many fascinating properties which can be seen neither from the large graphene sheet nor from the bulk graphite. One of such properties is the edge-selective generation of the Dirac-Fermi polarons (DFPs) with unexpectedly low effective mass, extremely high mobility [1,2], non-zero spin [3–6], and the spin quantum Hall effect [7,8]. Considering the additional attribute of the locally-anchored dipoles induced by the densely and locally entrapped core electrons, as identified recently [9], the DFPS should also include the nature of polarization. The generation of DFPS surrounding an atomic vacancy at a graphite surface [10,11],

at a zigzag edge of monolayer graphite terrace [12,13] and graphene nanoribbons (GNRs) [14,15] have been identified using scanning tunneling microscopy/spectroscopy (STM/S). The generation of DFPS makes GNR one kind of two-dimensional topological insulators [16] that have potentially revolutionary impact to the next-generation devices in electronics and spintronics [17–19]. However, challenging issues remain open for exploration as discussed as follows.

Firstly, the mechanism of the edge-discriminative generation of the DFPS remains a puzzle. The DFPS have been identified as a high electronic protrusion in morphology and a resonant peak at Fermi energy ( $E_F$ ) in spectroscopy by STM/S from the defects in identical hexagonal sublattice (atomic vacancy at graphite surface and zigzag-GNR (ZGNR) edges). DFPS

\* Corresponding author at: School of Electrical and Electronic Engineering, Nanyang Technological University, Singapore 639798, Singapore. Fax: +65 68733318.

E-mail address: [ecqsun@ntu.edu.sg](mailto:ecqsun@ntu.edu.sg) (C.Q. Sun).

0008-6223/\$ - see front matter © 2011 Elsevier Ltd. All rights reserved.

doi:10.1016/j.carbon.2011.04.064

can hardly be resolved at a clean graphite surface, the interior of GNR, or the edge of an armchair-GNR (AGNR). The charge density fluctuations associated with DFPs have been attributed to charge-donating impurities below the graphene surface, which induce standing wave patterns due to unexpected back-scattering of the fermions [20]. The interlayer interaction was suggested to play a crucial role in deriving the DFPs [21]. This mechanism applies only to graphene of two layers or more where interface interaction is involved. It is highly desired to clarify why the DFPs generate preferentially at the edge of a single-layer ZGNR or an atomic vacancy rather than at the edge of an AGNR or a reconstructed ZGNR (rec-ZGNR) [22].

Secondly, the magnetic properties of DFPs are very complicated and the values of the momentum remain uncertain. The occurrence of spin polarization to a ZGNR edge was firstly demonstrated by Fujita et al. [23,24], and confirmed by subsequent density-functional theory (DFT) calculations [25,26]. The GNRs show striking contrast in the electronic states depending on the shape of the edge [23]. Very weak onsite Coulomb repulsion can even induce finite magnetization about  $0.2\mu_B$  of an edge atom. The  $\mu_B$  is the Bohr magneton. A considerably large ZGNR edge magnetism of  $1.28\mu_B$  has also been derived in computations [27]. The presence of magnetism also depends on the shape, the density, and the sites of carbon atomic vacancies [5,28], structure defects [29–31], the position of hydrogen termination [4], and the spin polarization of *p* orbital [32]. Recently, we proposed that the magnetism of defects in the solids containing neither transition metals nor rare earth ions arises from the polarization of the unpaired nonbonding electrons by the under-coordination-induced densely, deeply, and locally entrapped bonding and core electrons or by the lone pair of electrons of N, O, and F [9]. Computational confirmation and clarification of this proposal of the local dipole formation with non-zero spin at different edges are necessary for improving the understanding of the DFPs.

Thirdly, the role of hydrogenation played in modulating the spin density of the DFPs is under debate. From the tight binding (TB) and the DFT calculations, Yazyev and Helm [28] concluded that the ferromagnetism in the GNR can only be induced at the single-atom defects and that the defect magnetism can be lowered from 1.17 to  $1.0\mu_B$  by hydrogenation. Another calculation [4] showed that the site-dependently unsaturated hydrogenation amplifies the magnetic momen-

tum of the GNR defect, instead. Using positron annihilation and magnetic measurements in combination with DFT calculations, Yang et al. [11] found that the magnetic moments of the DFPs are correlated only to the vacancy defects. The vacancy has a spin value around  $1.0\mu_B$  and the spin density is associated with the dangling bond electron [32]. Clarification of the roles of hydrogenation on the magnetic modulation of DFPs is necessary.

In this contribution, we report our findings in attending to the aforementioned concerns and their interdependence. The work was carried out using a combination of the DFT, the TB method in mean-field Hubbard model [33–36], from the perspective of the bond order–length–strength (BOLS) correlation [37]. Results are further confirmed using photoelectron emission spectroscopy analysis.

## 2. Principle

The BOLS correlation theory indicates that the shorter and stronger bonds between under-coordinated atoms provide perturbation to the local Hamiltonian and hence the charge distribution at sites surrounding the vacancies or the edges. The dangling  $\sigma$ -bond at edges neither follow the energy dispersion nor occupy the allowed energy states defined by the bulk-Hamiltonian because of their weak binding energies at the 10 s meV level [9]. Instead, the Fermions follow the Dirac motion equation and add additional “impurity” states at Fermi level or nearby. Therefore, the energetic fermions arise from the polarization of the unpaired nonbonding electrons by the densely and locally entrapped ones in the valence band and below.

Theoretic reproductions of the elastic modulus enhancement [38–40], melting point depression of carbon nanotubes [39,41], layer-number- and strain-dependent Raman shift of GNR [42], the shift of C 1s binding energy of graphene, graphite, and diamond [43–45], and the width-dependence of the band gap expansion of AGNR [37] have confirmed the BOLS correlation theory consistently that the C–C bond at the GNR edge contracts by 30% from 0.154 to 0.107 nm with a 152% increase of bond energy [39] and the elastic modulus is 2.6 TPa [38,40]. For the 3-coordinated GNR interior atoms, the C–C bond contracts by 18.5% to 0.125 nm with a 68% increase of bond energy. Girit et al. [14] discovered that breaking a C–C bond of the 2-coordinated carbon atom near the monolayer-GNR vacancy requires 7.50 eV per bond that is 32%

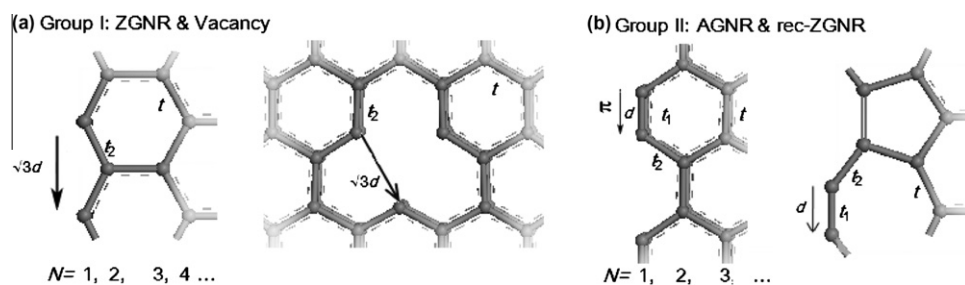


**Fig. 1** – Classification of the GNR edges and defects according to the distance between the dangling bond electrons along the edges. (a) Group I includes the edge of ZGNR (*N* indicates the counting of ribbon width; the numbers also mark the atomic position) and an atomic vacancy with dangling  $\sigma$ -bond in an identical  $\sqrt{3}d$  distance ( $d$  is the C–C bond-length). (b) Group II contains the edges of AGNR and rec-ZGNR with dangling  $\sigma$ -bond in alternative  $d$  and  $2d$  distance along the edges. The reconstructed edge consists of 7- and 5-atom rings. The overlap integrals are indicated as  $t$ ,  $t_1$  and  $t_2$ .

higher than the energy (5.67 eV/bond) required for breaking one bond between 3-coordinated carbon atoms in the interior of a suspended graphene sheet. A recent discovery [46] shows that the mechanical strength of graphene increases with the density of defects (the reconstructed 5- and 7-atom rings forming the grain boundaries), because of the particular strength of the ring bonds and their elongation dynamics. These findings provide further evidence for the BOLS prediction of the shorter and stronger bonds at GNR edges, vacancies and grain boundaries.

In the TB Hubbard model, the spin-polarized Hamiltonian can be expressed as:

$$H_\sigma = \sum_{i,\sigma} \Delta_i c_{i,\sigma}^\dagger c_{i,\sigma} + \sum_{(ij),\sigma} t_{ij} (f_{ij} c_{i,\sigma}^\dagger c_{j,\sigma} + f_{ij}^* c_{j,\sigma}^\dagger c_{i,\sigma}) + \sum_i U_i \hat{n}_{i,\sigma} \hat{n}_{i,-\sigma} \quad (1)$$

where  $i$  represents the  $i$ th atom and  $j$  the nearest neighbor;  $\sigma$  is the spin with sign. The  $t_{ij}$  is the overlap integral between the nearest neighbors and  $f_{ij}$  the periodic factor determined by the structure. As the onsite energy  $\Delta_i$  is the sum of the exchange integral and the eigen-energy of the  $p_z$  electron. The  $\Delta_D$  and  $t_D$  are the onsite energy and the overlap integral of dangling  $\sigma$ -bond electron, respectively. The last term is the Hubbard electron repulsion.

Supposing the  $U_i$  as a constant  $U$ , the  $k$ -dependent electron repulsion term within the mean-field approximation becomes,

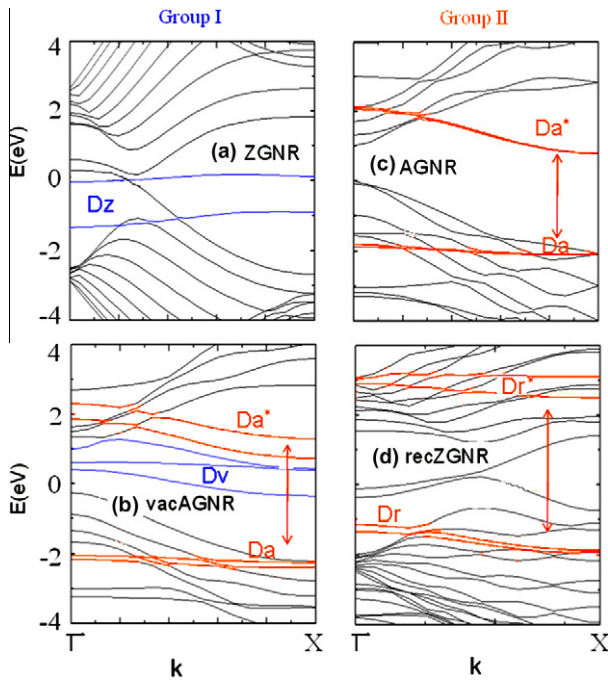


**Fig. 2 – Comparison of the DFT-derived energy dispersions of (a) ZGNR, (b) vac-AGNR, (c) AGNR and (d) rec-ZGNR. The  $D_z$  and  $D_v$  (in blue) represent the dangling  $\sigma$ -bond states of zigzag edge and atomic vacancy in group I, which are localized near the Fermi level ( $E_F$ ); The double  $D_a$  and  $D_r$  states (in orange) represent the bonding and anti-bonding states of armchair edge and rec-zigzag edge in group II, which are apart from the  $E_F$ . (For interpretation of the references to color in this figure legend, the reader is referred to the web version of this article.)**

$$H_U(k) = U \sum_{i,\sigma} \left[ \left( \hat{n}_{i,-\sigma} - \frac{1}{2} \right) c_{i,\sigma}^\dagger(k) c_{i,\sigma}(k) \right]$$

with

$$\langle \hat{n}_{i,\sigma} \rangle = \frac{1}{2\pi} \int_{-\pi}^{\pi} dk c_{i,\sigma}^\dagger(k) c_{i,\sigma}(k) \quad (2)$$

In the present BOLS-TB, we took the following relations of effective coordination number ( $z$ ), bond length ( $d$ ), single bond energy ( $E$ ), potential ( $V$ ) and overlap integral ( $t$ ) into consideration,

$$\begin{cases} d_i = C_z d_B = 2d_B \{1 + \exp[(12 - z_i)/(8z_i)]\}^{-1} & \text{(Bond contraction coefficient)} \\ E_i = E_B C_z^m & \text{(Bond energy)} \\ t_{ij}(z_i) = \langle \varphi_i(r) | V - V_i | \varphi_j(r) \rangle \alpha E_i(z_i) & \text{(Overlap integral)} \\ \frac{t_1}{t} = \frac{C_z(2)^{-2.56}}{C_z(3)^{-2.56}} = 1.49 & \text{(Bare edge integral)} \\ \frac{t_2}{t} = \frac{C_z(2.5)^{-2.56}}{C_z(3)^{-2.56}} = 1.17 & \text{(Bare edge-interior integral)} \\ \frac{t_3}{t} = C_{zH}^{-2.56} = 1.11 & \text{(H-edge integral)} \end{cases} \quad (3)$$

$C_z$  is the bond contraction coefficient. The  $t_1$  and  $t_2$  (reduced from  $t_{ij}$  if the  $t$  for the bulk is taken as reference) at the edge, as shown in Fig. 1, is proportional to the bond energy at equilibrium, therefore,  $t_1 > t_2 > t = 2.4$  eV because of the under-coordination induced bond strengthening. Fig. 1 also illustrates that the atomic vacancy and the typically edged GNRs that we concerned can be grouped as I and II according to the distance between the dangling bond electrons along the edges. A quasi-triple-bond is suggested to be formed between the nearest edge atoms in group II, since the shorter separation  $d$  will become even shorter by up to 30% due to BOLS correlation, which demolishes the nature of the dangling  $\sigma$ -bond.

### 3. Computational and experimental details

In the BOLS-TB calculations, the onsite energy  $\Delta_i$  for the  $p_z$  electrons and the  $\Delta_D$  for the dangling  $\sigma$ -bond electrons in Eq. (1) are identical for the elemental carbon and reduced to 0 eV as a reference. The overlap integral  $t_D$  between the dangling  $\sigma$ -electron orbital and the  $p_z$  orbital of the nearest neighbors is about  $-0.5$  eV, since the orbitals have different symmetries in the  $z$ -direction [36]. The onsite electron–electron repulsion energy, Hubbard  $U$ , is set uniformly as 2.0 eV [28]. The spin-up and spin-down electronic structures are solved self-consistently.

In order to clarify the local charge distribution and polarization of the bare and the hydrogenated edge atoms, DFT calculations were also performed using the CASTEP code [47]. The GNR is modeled with a 1 nm vacuum slab in both the  $y$  and the  $z$  directions. The CA-PZ [48,49] functional form in the local density approximation is chosen to approximate the exchange–correlation energy. The spin-polarized geometry optimization are converged with the tolerances of  $10^{-5}$  eV/atom, the maximum force of 0.03 eV/Å, maximum stress of 0.05 GPa, and the maximum displacement of 0.001 Å.

Using the standard X-ray photoelectron spectroscopy (XPS) and the standard process of experiment, we collected the XPS data of graphite surfaces at 75° and 25° before and after the surface being conditioned using energetic Ar<sup>+</sup> spray. Upon the spectral peak area normalization and background correction, we then differentiated the spectra to get the atomic-scale, zone-selective information of the bonding and electronic

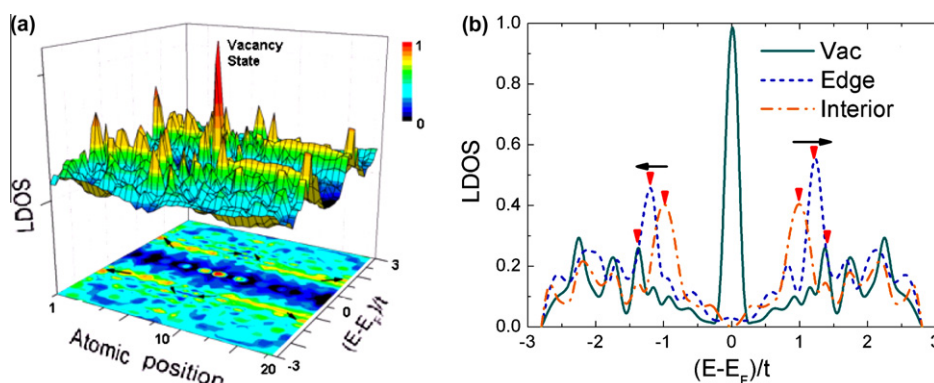


**Fig. 3 – (a)** The BOLS-TB derived LDOS of the H-vac-AGNR shows the  $E_F$  resonant peak, being consistent with that observed from both the graphite surface vacancy [10] and the ZGNR edge [24]. The atomic position denotes the position where the  $p_z$  electron posits, as defined in Fig. 1, at the GNR unit cell. **(b)** The polarization and entrapment is more pronounced for the vacancy than that at the edge and at the GNR interior as arrows indicated.

dynamics. We called this process atomistic photoelectron distillation spectroscopic (APDS) analysis. The APDS of C 1s band purifies the surface and the defect states within the limit of at most two atomic diameter distances.

## 4. Results and discussion

### 4.1. Effect of interaction between edge dangling $\sigma$ -bonds on DFPs

As expected, the DFT-derived electronic structures of ZGNR, vac-AGNR (Atomic vacancy is set in the middle of an AGNR since the armchair edge has seldom disturbance on the presence of vacancy states), AGNR and rec-ZGNR in Fig. 2 support the proposal of the formation of DFPs in Group I and the formation of quasi-triple-bond in group II. Group I exhibits two and three sharp  $\sigma$ -bond states denoted, respectively, as  $D_z$  and  $D_v$  near to  $E_F$ , varying almost linearly with the wave vector  $k$ ; whereas, group II manifests two separate states aside and located far away from the  $E_F$  denoted as  $D_a$  and  $D_r$ . The latter indicates that the interaction between the nearest  $\sigma$ -bond elections in group II are strong enough to make the dangling-bond energy bands split into a bonding and an anti-bonding band, which is a symptom of the formation of quasi-triple-bond between the edge atoms. Therefore, the formation of quasi-triple-bond determined by the structure associated with the under-coordination effect play a significant role on the vacancy- and edge-selective generation of DFPs.

### 4.2. Vacancy states and quantum entrapment

The BOLS-TB derived local density-of-states (LDOS) of a hydrogenated vac-AGNR (H-vac-AGNR) with ribbon width  $N = 20$  is shown in Fig. 3. A sharp resonant peak at vacancy site near  $E_F$  can be observed in Fig. 3(a), which is consistent with that identified experimentally from graphite surface vacancy [10]. Moreover, the arrows in Fig. 3(b) indicate that the separation between the bonding and the anti-bonding bands of the  $p_z$  electrons increases in magnitude from the inner to the edge and then to the vacancy sites. This observation indicates that the extents of the entrapment of the bonding states and the polarization of the anti-bonding states increase with

the reduction of atomic coordination number, complying with the BOLS theory expectations. The coordination trend of the quantum entrapment is also consistent with what resolved from the C 1s core band [45]. The polarization of the unpaired nonbonding electrons by the densely entrapped bonding electrons is the nature and sequence of the generation of DFP.

### 4.3. Magnetism of DFPs with and without hydrogenation

The local spin density of states (LSDOS) difference between up and down of the considered edges with and without hydrogenation and the spin electron density in real space are compared in Fig. 4. The LSDOS is the net spin density of occupied states distributed in energy space under the  $E_F$ , which shows the resultant contribution of the  $p_z$  electrons and the dangling  $\sigma$ -bond electrons. The magnetic momentum derived from both the BOLS-TB and the DFT calculations are consistent and complementary. Results are understood as follows:

- (i) Edges in group I demonstrate a high spin density ( $0.7\text{--}1.0$  electron/ $\text{\AA}^3$ ) in an asymmetric dumbbell-shape, indicating the dominance of the polarized unpaired dangling  $\sigma$ -bond electrons ( $D_v, D_z$ ).
- (ii) Edges in group II (including rec-ZGNR edge without shown in the figure) show an extremely low spin density ( $<0.05$  electron/ $\text{\AA}^3$ ) indicating the formation of quasi-triple-bond of edge atoms that pairs up the spins and hence cripples the magnetic momentum.
- (iii) Hydrogenation reduces the spin density of group I to  $0.1\text{--}0.3$  electron/ $\text{\AA}^3$  and unifies the orientations of the adjacent spin density from antiferromagnetic to paramagnetic. The residual spherical-shaped spin density represents the remnant of the entrapped  $p_z$  electron. The formation of a C-H bond renders the dangling  $\sigma$ -bond electron without influencing the  $p_z$  electron.

### 4.4. APDS verification

One may note that the DFPs generated at the atomic vacancy of a graphite surface [10] are the same to those generated at the ZGNR edge [7] despite the resonant peak sharpness. The

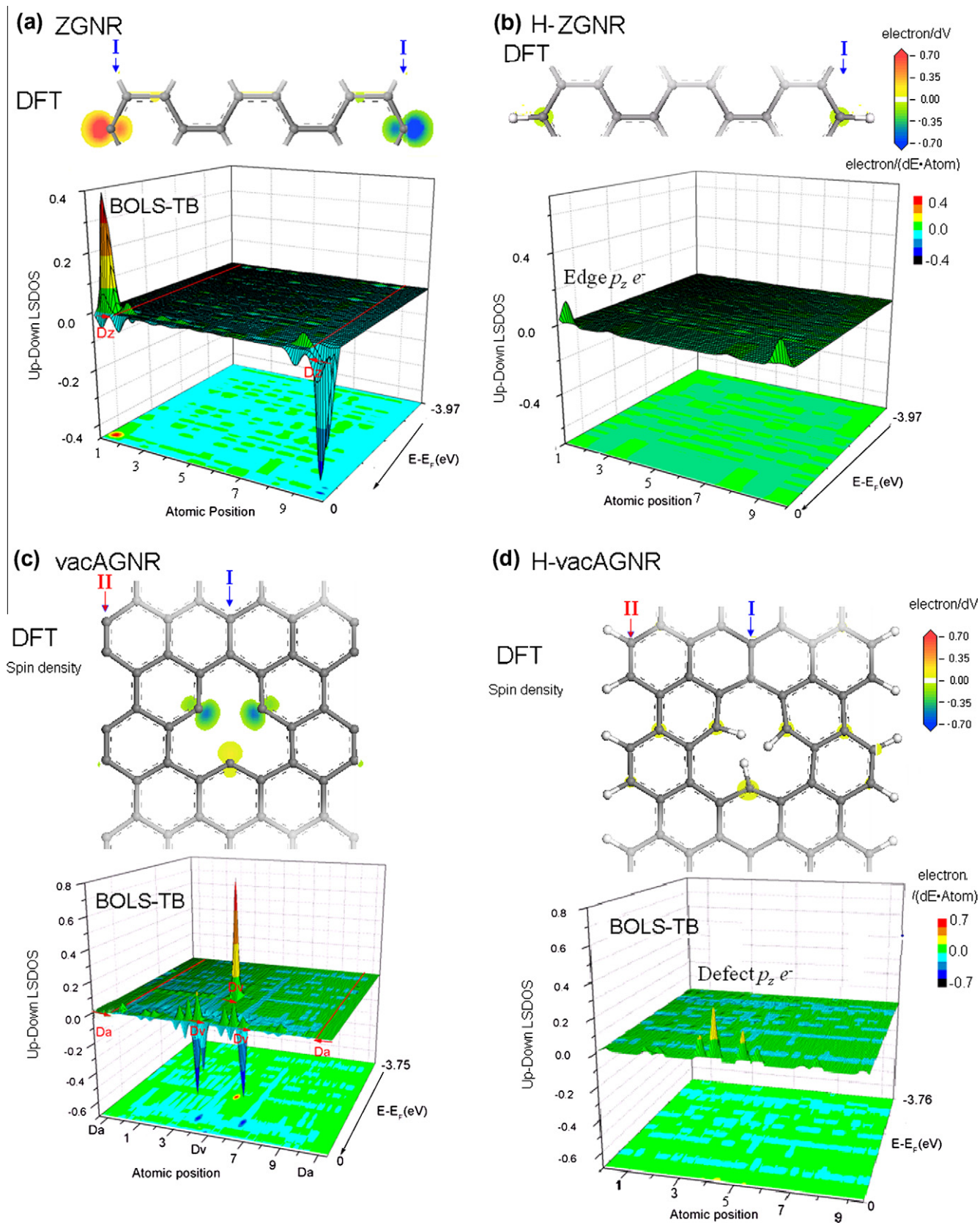
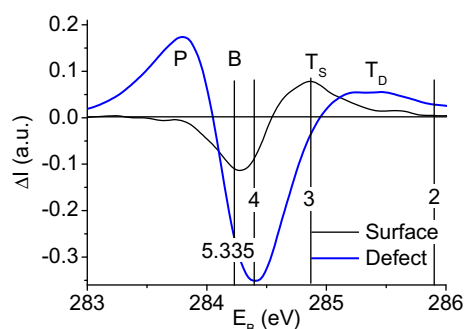


Fig. 4 – Comparison of the DFT-derived spin electron density and the BOLS-TB derived difference LSDOS for (a) ZGNR, (b) H-ZGNR, (c) vac-AGNR and (d) H-vac-AGNR. The dangling  $\sigma$ -bonds of group I ( $D_z$  and  $D_v$ ) and the  $p_z$  electron, contributes to a strong dumbbell-shaped magnetism and a weak spherical spin, respectively. Hydrogenation interacts and pairs up the dangling  $\sigma$ -bond electron other than the  $p_z$  electrons.



**Fig. 5** – Comparison of the purified XPS C 1s spectrum of graphite surface with and without vacancy defects showing that bonds near to defects are shorter and stronger than those at the surface [9]. The P,  $T_S$ , and  $T_D$  denotes, respectively, the DFPs screened, undercoordination-induced quantum entrapment states of the outermost two atomic layers of surface skin ( $z = 3.2$ ) and sites surrounding vacancy defects ( $z = 2.5$ ); B indicates the spectral component of bulk graphite ( $z = 5.335$ ). The valleys centered at  $284.2(z = 5.335)$  and  $284.4(z = 4)$  correspond, respectively, to the removed obvious graphite bulk and the surface information. Indicated numbers are the effective  $z$  values.

peak sharpness is subject to experimental conditions such as the STM/S tip sharpness and operating temperatures. This fact allowed us to identify the physical origin and the force for the retention of DFPs by probing the bonds and electrons at the atomic-scaled zones surrounding the surface DFPs because the signal from graphite vacancies is much stronger than that from GNR edges.

The APDS results shown in Fig. 5 demonstrate the BOLS-TB expected surface ( $T_S$ ) and defect ( $T_D$ ) entrapment states at the bottom edge of the C 1s band [9]. The separation between the entrapped states and the reference point (the energy level of an isolated atom at 258.57 eV) [45] is proportional to the cohesive energy per bond at equilibrium. Therefore, it has been clarified unambiguously that the defect bonds are shorter and stronger than those at the surface and the surface bonds are shorter and stronger than those in the bulk (spectral valley). The additional peak P at the top edge of the C 1s band derived by defects arises from screening a splitting of the crystal potential by the DFPs. Results confirmed therefore that the DFPs arise from the polarization of the dangling bond electrons by the deeply and densely entrapped local bonding electrons.

## 5. Conclusions

A combination of the BOLS-TB and DFT calculations and photoelectron measurements clarified the puzzles posed in the beginning of the presentation as follows:

Firstly, the graphitic DFPs arise from the polarization of the dangling  $\sigma$ -bond electrons by the locally and deeply entrapped core and bonding electrons at atomic vacancy and the edges of ZGNR.

Secondly, the preference of generation of DFPs with a high-spin density at the atomic vacancy and at the ZGNR edge is determined by the isolation and polarization of the unpaired dangling  $\sigma$ -bond electrons of the under-coordinated carbon

atoms. The shorter separation between the dangling  $\sigma$ -bond electrons along the AGNR and rec-ZGNR edges promotes the quasi-triple-bond formation and thus the polarization of the dangling bond electrons is prevented.

Finally, the hydrogenation offsets the spin of the dangling  $\sigma$ -bond electron rather than that of the entrapped  $p_z$  electron. Thus, in a system like ZGNR edge, where the dangling  $\sigma$ -bond electrons present, hydrogenation will cripple the local magnetism significantly.

## REFERENCES

- [1] Brey L, Fertig HA. Electronic states of graphene nanoribbons studied with the Dirac equation. *Phys Rev B* 2006;73(23):235411.
- [2] Novoselov KS, Geim AK, Morozov SV, Jiang D, Katsnelson MI, Grigorieva IV, et al. Two-dimensional gas of massless Dirac fermions in graphene. *Nature* 2005;438(7065):197–200.
- [3] Cervenka J, Katsnelson MI, Flipse CFJ. Room-temperature ferromagnetism in graphite driven by two-dimensional networks of point defects. *Nat Phys* 2009;5(11):840–4.
- [4] Lehtinen PO, Foster AS, Ma Y, Krasheninnikov AV, Nieminen RM. Irradiation-induced magnetism in graphite: a density functional study. *Phys Rev Lett* 2004;93(18):187202.
- [5] Palacios JJ, Fernández-Rossier J, Brey L. Vacancy-induced magnetism in graphene and graphene ribbons. *Phys Rev B* 2008;77(19):195428.
- [6] Pereira VM, Guinea F, Lopes dos Santos JMB, Peres NMR, Castroneto AH. Disorder induced localized states in graphene. *Phys Rev Lett* 2006;96(3):036801.
- [7] Enoki T, Kobayashi Y, Fukui KI. Electronic structures of graphene edges and nanographene. *Int Rev Phys Chem* 2007;26(4):609–45.
- [8] Soldano C, Mahmood A, Dujardin E. Production, properties and potential of graphene. *Carbon* 2010;48(8):2127–50.
- [9] Sun CQ. Dominance of broken bonds and nonbonding electrons at the nanoscale. *Nanoscale* 2010;2(10):1930–61.
- [10] Ugeda MM, Brihuega I, Guinea F, Gómez-Rodríguez JM. Missing atom as a source of carbon magnetism. *Phys Rev Lett* 2010;104(9):096804.
- [11] Yang XM, Xia HH, Qin XB, Li WF, Dai YY, Liu XD, et al. Correlation between the vacancy defects and ferromagnetism in graphite. *Carbon* 2009;47(5):1399–406.
- [12] Li G, Andrei EY. Observation of Landau levels of Dirac fermions in graphite. *Nat Phys* 2007;3(9):623–7.
- [13] Matsui T, Kambara H, Niimi Y, Tagami K, Tsukada M, Fukuyama H. STS observations of Landau levels at graphite surfaces. *Phys Rev Lett* 2005;94:226403.
- [14] Girit CÖ, Meyer JC, Erni R, Rossell MD, Kisielowski C, Yang L, et al. Graphene at the edge: stability and dynamics. *Science* 2009;323(5922):1705–8.
- [15] Niimi Y, Kambara H, Fukuyama H. Localized distributions of quasi-two-dimensional electronic states near defects artificially created at graphite surfaces in magnetic fields. *Phys Rev Lett* 2009;102(2):026803–26804.
- [16] Zazunov A, Kundu A, Hütten A, Egger R. Magnetic scattering of Dirac fermions in topological insulators and graphene. *Phys Rev B* 2010;82(15):155431.
- [17] Son Y-W, Cohen ML, Louie SG. Half-metallic graphene nanoribbons. *Nature* 2006;444(7117):347–9.
- [18] Zhang Y, Tan Y-W, Stormer HL, Kim P. Experimental observation of the quantum Hall effect and Berry's phase in graphene. *Nature* 2005;438(7065):201–4.
- [19] Zeng M, Shen L, Su H, Zhang C, Feng Y. Graphene-based spin logic gates. *Appl Phys Lett* 2011;98(9):092110–3.

- [20] Zhang YB, Brar VW, Girit C, Zettl A, Crommie MF. Origin of spatial charge inhomogeneity in graphene. *Nat Phys* 2009;5(10):722–6.
- [21] Ferro Y, Allouche A. Interpretation of STM images of graphite with an atomic vacancy via density-functional calculations of electronic structure. *Phys Rev B* 2007;75(15):155438.
- [22] Koskinen P, Malola S, Häkkinen H. Evidence for graphene edges beyond zigzag and armchair. *Phys Rev B* 2009;80(7):073401.
- [23] Fujita M, Wakabayashi K, Nakada K, Kusakabe K. Peculiar localized state at zigzag graphite edge. *J Phys Soc Jpn* 1996;65:1920.
- [24] Nakada K, Fujita M, Dresselhaus G, Dresselhaus MS. Edge state in graphene ribbons: nanometer size effect and edge shape dependence. *Phys Rev B* 1996;54(24):17954.
- [25] Okada S, Oshiyama A. Magnetic ordering in hexagonally bonded sheets with first-row elements. *Phys Rev Lett* 2001;87(14):146803.
- [26] Son YW, Cohen ML, Louie SG. Energy gaps in graphene nanoribbons. *Phys Rev Lett* 2006;97(21):216803.
- [27] Lee H, Son Y-W, Park N, Han S, Yu J. Magnetic ordering at the edges of graphitic fragments: Magnetic tail interactions between the edge-localized states. *Phys Rev B* 2005;72(17):174431.
- [28] Yazyev OV, Helm L. Defect-induced magnetism in graphene. *Phys Rev B* 2007;75(12):125408.
- [29] Ma S, Xia JH, Srikanth V, Sun X, Staedler T, Jiang X, et al. Magnetism of amorphous carbon nanofibers. *Appl Phys Lett* 2009;95(26):263105.
- [30] Xu B, Yin J, Xia YD, Wan XG, Jiang K, Liu ZG. Electronic and magnetic properties of zigzag graphene nanoribbon with one edge saturated. *Appl Phys Lett* 2010;96(16):163102.
- [31] Zanolli Z, Charlier JC. Spin transport in carbon nanotubes with magnetic vacancy-defects. *Phys Rev B* 2010;81(16):165406.
- [32] Volnianska O, Boguslawski P. Magnetism of solids resulting from spin polarization of p orbitals. *J Phys: Condens Matter* 2010;22(7):073202.
- [33] Hubbard J. Electron correlations in narrow energy bands. *Proc R Soc London Ser A* 1963;276:238.
- [34] Reich S, Maultzsch J, Thomsen C, Ordejo P. Tight-binding description of graphene. *Phys Rev B* 2002;66(3):035412.
- [35] Wang ZF, Li Q, Zheng H, Ren H, Su H, Shi QW, et al. Tuning the electronic structure of graphene nanoribbons through chemical edge modification: a theoretical study. *Phys Rev B* 2007;75(11):113404–6.
- [36] Zheng F, Sasaki KI, Saito R, Duan W, Gu BL. Edge states of zigzag boron nitride nanoribbons. *J Phys Soc Jpn* 2009;78(7):074713.
- [37] Zhang X, Kuo J-I, Gu M, Bai P, Sun CQ. Graphene nanoribbon band-gap expansion: broken-bond-induced edge strain and quantum trap depression. *Nanoscale* 2010;2:2160–3.
- [38] Falvo MR, Clary GJ, Taylor RM, Chi V, Brooks FP, Washburn S, et al. Bending and buckling of carbon nanotubes under large strain. *Nature* 1997;389(6651):582–4.
- [39] Sun CQ, Bai HL, Tay BK, Li S, Jiang EY. Dimension, strength, chemical and thermal stability of a single C–C bond in carbon nanotubes. *J Phys Chem B* 2003;107:7544–6.
- [40] Wong EW, Sheehan PE, Lieber CM. Nanobeam mechanics: elasticity, strength, and toughness of nanorods and nanotubes. *Science* 1997;277(5334):1971–5.
- [41] An B, Fukuyama S, Yokogawa K, Yoshimura M. Surface superstructure of carbon nanotubes on highly oriented pyrolytic graphite annealed at elevated temperatures. *Jpn J Appl Phys* 1998;37(Part 1, No. 6B):3809–11.
- [42] Ni ZH, Yu T, Lu YH, Wang YY, Feng YP, Shen ZX. Uniaxial strain on graphene: Raman spectroscopy study and band-gap opening. *ACS Nano* 2008;2(11):2301–5.
- [43] Balasubramanian T, Andersen JN, Walldén L. Surface-bulk core-level splitting in graphite. *Phys Rev B* 2001;64:205420.
- [44] Kim KJ, Lee H, Choi JH, Youn YS, Choi J, Lee H, et al. Scanning photoemission microscopy of graphene sheets on SiO<sub>2</sub>. *Adv Mater* 2008;20(19):3589–91.
- [45] Sun CQ, Sun Y, Nie YG. Coordination-resolved C–C bond length and the C 1s binding energy of carbon allotropes and the effective atomic coordination of the few-layer graphene. *J Phys Chem C* 2009;113:16464–7.
- [46] Grantab R, Shenoy VB, Ruoff RS. Anomalous strength characteristics of tilt grain boundaries in graphene. *Science* 2010;330(6006):946–8.
- [47] Clark SJ, Segall MD, Pickard CJ. First principles methods using CASTEP. *Zeitschrift fuer kristallographie (Crystalline Materials)* 2005;220(5–6):567–70.
- [48] Ceperley DM, Alder BJ. Ground state of the electron gas by a stochastic method. *Phys Rev Lett* 1980;45:566–9.
- [49] Perdew JP, Zunger A. Self-interaction correction to density-functional approximations for many-electron systems. *Phys Rev B* 1981;23:5048–79.